MOLECULAR AND CELLULAR BIOLOGY, Feb. 1996, p. 724–734 Vol. 16, No. 2
0270-7306/96/$04.00+0

Autoactivation by a *Candida glabrata* Copper Metalloregulatory Transcription Factor Requires Critical Minor Groove Interactions

KEITH A. KOCH AND DENNIS J. THIELE*

Department of Biological Chemistry, The University of Michigan Medical School, Ann Arbor, Michigan 48109-0606

Received 1 September 1995/Returned for modification 19 October 1995/Accepted 7 November 1995

Rapid transcriptional autoactivation of the *Candida glabrata AMT1* copper metalloregulatory transcription factor gene is essential for survival in the presence of high extracellular copper concentrations. Analysis of the interactions between purified recombinant AMT1 protein and the *AMT1* promoter metal regulatory element was carried out by a combination of missing-nucleoside analysis, ethylation interference, site-directed mutagenesis, and quantitative in vitro DNA binding studies. The results of these experiments demonstrate that monomeric AMT1 binds the metal regulatory element with very high affinity and utilizes critical contacts in both the major and minor grooves. A single adenosine residue in the minor groove, conserved in all known yeast Cu metalloregulatory transcription factor DNA binding sites, plays a critical role in both AMT1 DNA binding in vitro and Cu-responsive *AMT1* gene transcription in vivo. Furthermore, a mutation in the AMT1 Cu-activated DNA binding domain which converts a single arginine, found in a conserved minor groove binding domain, to lysine markedly reduces AMT1 DNA binding affinity in vitro and results in a severe defect in the ability of *C. glabrata* cells to mount a protective response against Cu toxicity.

The survival of all organisms under environmental stress is dependent on the capacity to both sense stress signals and mount the appropriate protective or adaptive response. In many cases, environmental changes are monitored through membrane-associated receptor molecules which transmit these signals, via protein kinase cascades or other signalling pathways, to activate the transcription machinery on stress-responsive target genes. The metal copper (Cu) poses a unique environmental stress, since Cu is both an essential and yet a toxic cellular constituent. As a redox metal, Cu is utilized by a large number of enzymes, such as Cu,Zn superoxide dismutase, lysyl oxidase, cytochrome oxidase, and dopamine β-hydroxylase, as a catalytic cofactor (34). Ironically, this same redox activity allows Cu to undergo Haber-Weiss and Fenton-type chemistry resulting in the production of cytotoxic reactive oxygen species which cause direct protein oxidation, lipid peroxidation, and cleavage of DNA and RNA (22, 23). Furthermore, as demonstrated for the DNA binding activity of the estrogen receptor, Cu may displace other metals such as zinc, thereby destroying normal biological activity (38). Therefore, cellular Cu levels must remain within homeostatic boundaries to allow sufficient Cu to accumulate to drive essential biochemical reactions and yet prevent the accumulation of Cu to cytotoxic levels.

In eukaryotic organisms, a major protective mechanism against Cu toxicity is mediated by the transcriptional activation of a family of genes encoding low-molecular-weight, cysteine-rich metal-binding proteins known as metallothioneins (MTs). This transcriptional activation involves *cis*-acting metal-responsive elements (MREs), found in multiple copies in MT gene promoters, and metal-responsive transcription factors (25, 37, 45). Although for higher eukaryotes the precise mechanisms whereby cells sense elevated levels of Cu are not well understood, studies with yeast cells have demonstrated that the same molecule both senses and responds to increases in environmental Cu levels to activate MT gene transcription (25, 37, 45). These molecules, designated Cu metalloregulatory transcription factors (CuMRTFs), have been identified for the baker's yeast *Saccharomyces cerevisiae* (*ACE1*) and the opportunistic yeast *Candida glabrata* (*AMT1*), and their genes have been cloned (10, 44, 51). The ACE1 and AMT1 proteins harbor an amino-terminal, cysteine-rich, positively charged DNA binding domain which is activated by the binding of multiple Cu(I) ions, via a cysteine thiolate polynuclear cluster, to bind to MRE sequences in an inducible fashion. This Cu(I) coordination, which is thought to occur cooperatively, provides the thermodynamics to drive a conformational alteration in the CuMRTF DNA binding domain, thereby activating sequence-specific DNA binding (18, 19, 30). Purified yeast CuMRTFs bind as monomers to MREs, which are unrelated in sequence to the MREs found in higher eukaryotes (25, 45). Once bound, CuMRTFs rapidly and potently activate target gene transcription via a highly acidic carboxy-terminal transcriptional activation domain (29). To date, the known target genes for yeast CuMRTFs include MTs and the gene encoding Cu,Zn superoxide dismutase (*SOD1*) in *S. cerevisiae* (11, 19, 21, 44, 49). Although most yeast MT gene promoters harbor multiple MREs and are strongly activated in response to Cu, the *S. cerevisiae CRS5* gene, encoding an MT isoform, and the *SOD1* gene harbor a single MRE and are only modestly transcriptionally activated by CuACE1 (11, 21). The observation that deletion of either the *ACE1* gene or the *AMT1* gene renders yeast cells exquisitely sensitive to Cu toxicity underscores the importance of CuMRTFs in sensing elevations in Cu levels and initiating the appropriate detoxification response (44, 49).

Unlike the *S. cerevisiae ACE1* gene, which is constitutively expressed, the *AMT1* gene in *C. glabrata* is induced 15- to 20-fold in response to Cu via a transcriptional autoactivation mechanism that requires AMT1 and a single MRE in the *AMT1* promoter (52). *AMT1* transcriptional autoactivation occurs extremely rapidly and is followed by the transcriptional activation of a family of *C. glabrata* MT genes including *MT-1*,

* Corresponding author. Phone: (313) 763-5717. Fax: (313) 763-4581. Electronic mail address: DTHIELE@UMICH.EDU.

MT-IIa, and *MT-IIb* (49, 52). An *AMT1* allele defective in transcriptional autoactivation results in reduced MT gene transcription, lower steady-state levels of MT protein, and consequently a reduced ability of *C. glabrata* cells to survive in the presence of elevated Cu concentrations (52). Therefore, the potent Cu-responsive *AMT1* gene autoactivation elicited by the single *AMT1* promoter MRE provides an excellent system to analyze the details of CuMRTF-MRE interactions, in terms of both protein-DNA interactions and the transcriptional and biological consequences of mutations in AMT1 or the MRE. Because of the essential and toxic nature of Cu, it is critical to understand how cells respond to fluctuations in Cu levels to maintain homeostatic control.

In this report, we have utilized several approaches to define the nature of the molecular interactions between the AMT1 protein and the *AMT1* MRE. We demonstrate that AMT1 makes critical MRE interactions in the major and minor grooves and that a single nucleotide in the minor groove, perfectly conserved in all known yeast MREs, is critical for both DNA binding in vitro and *AMT1* gene transcriptional activation in vivo. Furthermore, an arginine residue in the AMT1 Cu-activated DNA binding domain, embedded within a region similar to other known minor groove binding motifs, plays a critical role in high-affinity DNA binding in vitro and in mounting a normal Cu detoxification response in vivo. Taken together, these studies demonstrate that this unique class of toxic-metal-sensing transcription factors utilizes important contacts in both the major and minor grooves of the MRE for transcriptional responses to elevated environmental copper concentrations.

MATERIALS AND METHODS

Strains and growth conditions. Two previously described *C. glabrata* uracil-auxotrophic strains, Q and an *AMT1* disruption (*amt1-1*) strain (49), were used in this study. Strains were grown at 30°C in rich medium (1% yeast extract, 2% Bacto Peptone, 2% dextrose) (YPD) or synthetic complete medium lacking uracil (SC-ura) for strains transformed with plasmids bearing the *URA3* gene, as previously described (3, 40). The Q strain was used as the recipient for episomal plasmids bearing the wild-type or mutant *AMT1-lacZ* reporter genes. The *amt1-1* strain was the parental strain used for the integration of wild-type and mutant full-length *AMT1* genes at the *ura3*$^-$ locus to generate isogenic strains by transformation and homologous recombination (50). Copper induction of transcription in the Q strain was initiated by the addition of 100 μM $CuSO_4$ to cells grown to mid-logarithmic phase (optical density at 650 nm = 1.5 to 2.0) in SC-ura medium. The *Escherichia coli* strain XL-1 blue was used for the construction and maintenance of plasmids by standard techniques (3).

Plasmids. Because of the low level of AMT1 protein expressed from the wild-type coding sequence in *E. coli*, a chimeric expression plasmid (pET-AF5) having the first 115 codons of *AMT1* optimized for translation in *E. coli* (48) fused to the natural *AMT1* codons 116 through 265 was constructed. The DNA containing the synthetic amino-terminal 115 codons of *AMT1* optimized for *E. coli* was produced at Warner Lambert Parke-Davis (Ann Arbor, Mich.). To construct an in-frame translational fusion to the wild-type carboxyl-terminal coding sequence, an *Afl*II site was engineered into the synthetic coding sequence by PCR mutagenesis using the oligonucleotide 5′-GTGGATCCTTAAGTTGT CTTT-3′. The PCR-amplified fragment containing the *Afl*II mutation was subcloned into pBluescript SK+ (Stratagene, La Jolla, Calif.), and the presence of the mutation with no other DNA sequence alterations was confirmed by dideoxy sequencing. The 345-bp *Nco*I-*Afl*II fragment was subsequently reconstituted with the wild-type *AMT1* carboxyl-terminal codons 116 to 265 in the vector pET-3d (42) to generate the full-length AMT1 expression plasmid pET-AF5.

To facilitate the study of interactions between recombinant AMT1 and the *AMT1* promoter MRE, the plasmid pAMNE, containing nucleotides spanning the region from position −253 to position −131 with respect to the transcriptional start in the *AMT1* promoter, was made. pAMNE contains a 122-bp *Dde*I-*Ssp*I fragment, which was made blunt ended by using the Klenow fragment of DNA polymerase I and subcloned into the *Eco*RV site of pBluescript SK+. To aid the analysis of interactions between AMT1 and *AMT1* promoter fragments harboring the mutations described in this paper, two oligonucleotides were synthesized for the PCR amplification of the *AMT1* promoter region from position −252 to position −107. The oligonucleotides PCR-ABS-1 (5′-CGCGGA TCCAGTGGCACT-3′) and PCR-ABS-2 (5′-CGCGAATTCAACTACTTGCC T-3′) were used to PCR amplify this region from the plasmids pKTP-1G, pKTP-1A, and pKTP-1C (described below) and a plasmid bearing a deletion of the 16-adenosine tract, pBZ12-A16Δ (provided by Zhiwu Zhu). The PCR products obtained were digested with *Bam*HI and *Eco*RI and cloned into the corresponding sites of pBluescript SK+. The resulting plasmids were designated pKTP-6G, pKTP-6A, pKTP-6C, and pΔAKD, respectively.

To analyze the effect of altering the base composition at position −195 in the *AMT1* promoter MRE on the ability of AMT1 to activate transcription from the *AMT1* promoter, site-directed mutagenesis was performed to mutate this position to the three other nucleotides. The oligonucleotide 5′-TCATGATAAGCT AANTTGGCTGACTTAAAAGTAGTGG-3′ was used in conjunction with the T7 primer to amplify 500-bp fragments containing all four possible bases at position −195 of the *AMT1* promoter from the plasmid pBZ-12. The plasmid pBZ-12 contains the 706-bp *Bgl*II-*Xho*I fragment of the *AMT1* gene cloned into the *Bam*HI and *Xho*I sites of pBluescript SK+. The resultant PCR products were digested with *Xho*I and cloned into the *Xho*I and *Eco*RV sites of pBluescript SK+. The DNA sequence spanning the *Bsp*HI-to-*Dra*I site was confirmed for each mutant by dideoxy sequencing, and this fragment was subsequently isolated and used to replace the equivalent *AMT1* promoter fragment in pBZ-12. The plasmids containing the *Bgl*II-*Xho*I fragment of the *AMT1* promoter with a G, A, or C in place of the T at position −195 on the coding strand were designated pKTP-1G, pKTP-1A, and pKTP-1C, respectively.

AMT1-lacZ fusion plasmids containing the wild-type or T-mutant *AMT1* promoter and the first 38 codons of *AMT1* fused in frame to the eight codon of the *E. coli lacZ* gene were constructed by a strategy described previously (52). The resultant *AMT1-lacZ* fusion plasmids having a pRS316 backbone were designated pKTP-8G, pKTP-8A, pKTP-8T, and pKTP-8C, which correspond to the G mutant, A mutant, wild type, and C mutant, respectively.

The plasmid pAIRP2 was constructed for the production of an antisense RNA probe for RNase protection analysis of *AMT1-lacZ* mRNA levels. The 214-bp *Rsa*I-to-*Xho*I fragment from the *AMT1* transcribed region was cloned into the *Eco*RV and *Xho*I sites of pBluescript SK+ to produce pAIRP2. *C. glabrata URA3* mRNA levels, used as a control for the amount of RNA used in the RNase protection analysis described below, were analyzed by using *URA3* antisense RNA generated from the plasmid pURP. The vector pURP contains the 254-bp *Hin*cII-*Dra*I fragment of the *C. glabrata URA3* (50) gene cloned into the *Hin*cII site of pBluescript SK+.

To assess the effects of the mutation of R-38 to K (R38K mutation) in AMT1 on in vitro DNA binding and in vivo copper resistance in the *amt1-1* background, plasmids pKTP-10R2K and pET-R2K were generated, respectively. To generate the R38K mutation, the oligonucleotide AMT1-R2K 5′-CCAAGGGGAAAAC CACCGACG-3′ was used in conjunction with the T7 primer to PCR amplify a 110-bp fragment from the plasmid pBZ-12, which was then subcloned into the *Sma*I and *Xho*I sites of pBluescript SK+. The sequence of the *Sty*I-to-*Xba*I fragment was confirmed by dideoxy sequencing, and this fragment was used to replace the equivalent wild-type fragment in plasmids pET-AMT1 and pAMT1::URA3 (50) to generate pET-R2K and pKTP-10R2K, respectively.

The plasmid pKTP-10R2K contains the full-length *AMT1 R38K* gene in a 2.5-kb *Bgl*II-*Asp*718 fragment cloned into plasmid pU(1)b, as described previously (50). For integration of the mutant gene in the *amt1-1* strain, pKTP-10R2K was linearized within the *URA3* gene by using *Stu*I. Competent *amt1-1* cells were made as previously described, and the linearized plasmid was used for transformation. Selection for transformants was carried out on SC-ura plates, and single-copy integrants at the *ura3*$^-$ locus were identified by Southern blotting (3).

Expression and purification of wild-type AMT1 and AMT1 R38K. The expression of full-length AMT1 and the AMT1 R38K in *E. coli* was carried out essentially as described previously for the expression of ACE1 (9). Briefly, fresh transformants of BL21(DE3)pLysS cells containing the plasmid pET-AF5, or pET-R2K, were grown to an optical density at 650 nm of 0.4 to 0.6 in 2× TY (2× TY is 1.5% Bacto Tryptone, 1% yeast extract, and 0.5% NaCl) containing 100 μg of ampicillin per ml and 30 μg of chloramphenicol per ml and were induced in the presence of 1 mM $CuSO_4$ with 0.4 mM IPTG (isopropyl-β-D-thiogalactopyranoside) for 2 h. Cells were harvested, resuspended in 1/50 of the original volume with 5 mM HEPES (*N*-2-hydroxyethylpiperazine-*N*′-2-ethanesulfonic acid; pH 7.9)–100 mM NaCl–5 mM dithiothreitol, and frozen at −80°C. The cells were thawed at 37°C in the presence of protease inhibitors (2 μg each of leupeptin, pepstatin A, and aprotinin per ml and 1 mM phenylmethylsulfonyl fluoride), lysed with a French pressure cell, and centrifuged (32,000 × *g* for 30 min at 4°C). The supernatant was heat treated at 70°C for 10 min and centrifuged as stated above. The heat-treated supernatant was loaded onto a heparin-agarose (Bio-Rad Laboratories, Hercules, Calif.) column equilibrated in 5 mM HEPES (pH 7.9)–100 mM NaCl–1 mM dithiothreitol (low-salt HEPES). This and all subsequent purification procedures were carried out at 4°C unless otherwise specified. The bound AMT1 was eluted with a linear NaCl gradient from 0.1 mM to 1.5 M in the buffer described above. The fractions containing AMT1 from the heparin column, detected by sodium dodecyl sulfate-polyacrylamide gel electrophoresis (SDS-PAGE), were pooled and dialyzed against low-salt HEPES buffer prior to being loaded onto an SP-Sepharose Fast Flow column (Pharmacia Biotech, Inc., Piscataway, N.J.). Elution of the bound AMT1 was performed under the conditions used for the heparin column. The fractions containing AMT1 were pooled and concentrated by using an Amicon stirred cell and YM3 (Amicon, Inc., Beverly, Mass.) membrane in the presence of 100% argon to maintain a reducing environment, and the concentrated protein was loaded onto

an S100 gel filtration column equilibrated in 25 mM Tris-HCl. The fractions containing AMT1 were pooled, and a final concentration of 5 mM β-mercaptoethanol and 10% glycerol were added prior to freezing at −80°C. The concentration of purified AMT1 was ascertained by amino acid analysis, and the purity was estimated to be >98% on the basis of amino-terminal sequence analysis of AMT1 in solution. The purified AMT1 was determined to be Cu saturated on the basis that additional exogenous Cu did not elevate AMT1's DNA binding activity in gel mobility shift experiments.

Quantitative in vitro DNA binding studies. DNA binding reaction mixtures contained 5 mM HEPES (pH 7.9), 100 mM NaCl, 5 mM $MgCl_2$, 1 mM dithiothreitol, and 10% glycerol (1× binding buffer) and the protein concentrations indicated in the figure legends. All probe and protein dilutions were made in 1× binding buffer. Binding reaction mixtures were equilibrated for 15 min at 25°C prior to being loaded onto a 6% native polyacrylamide gel (40:0.5 acrylamide/bis ratio), which had been preelectrophoresed for 30 min at 8 V/cm in 0.5× TBE (44.5 mM Tris, 44.5 mM borate, 1 mM EDTA [pH 8.0]). Samples were subjected to electrophoresis under the conditions described above until the bound and free species were sufficiently resolved.

Typically, 8 μg of the plasmid DNA was digested with *Eco*RI and *Hin*dIII (pAMNE), or *Eco*RI and *Bam*HI (pKTP-6G, pKTP-6A, and pKTP-6C), to release a 140-bp fragment containing the *AMT1* promoter MRE. After phenol-chloroform extraction and ethanol precipitation of the digest, the DNA was subjected to treatment with calf intestinal alkaline phosphatase. The dephosphorylated DNA was then labeled by using T4 polynucleotide kinase and [γ-^{32}P]ATP (3). The ^{32}P-labeled DNA was resolved on a 7.5% native polyacrylamide gel, and the labeled DNA fragment was isolated by electrophoretic transfer to DEAE paper (NA-45; Schleicher & Schuell, Keene, N.H.) in a Bio-Rad mini transfer apparatus with 0.5× TBE (190 mA for 1 h). Elution of the DNA from the membrane was carried out by using the high-salt NET (1.0 M NaCl, 0.1 mM EDTA, 20 mM Tris-HCl [pH 8.0]) buffer protocol provided by Schleicher & Schuell. The final DNA preparation was resuspended in 100 μl of 1× binding buffer.

Binding reaction mixtures (20 μl) contained 1× binding buffer and the range of protein concentrations indicated in the figure legends. Protein dilutions were carried out by sequential fourfold serial dilutions into 1× binding buffer. Probe concentrations were determined spectrophotometrically by A_{260} and maintained at <0.1 nM for apparent K_d ($K_{d,\mathrm{app}}$) determinations. Binding reaction mixtures were treated as described above, the gels were dried and exposed to a PhosphorImage screen (Molecular Dynamics, Sunnyvale, Calif.), and the radioactive bands were quantitated by using PhosphorImager SP and ImageQuant 3.3 software (Molecular Dynamics). The data derived from the PhosphorImage quantitation were plotted and analyzed by using Kaleidagraph software (Synergy Software, Reading, Pa.). The $K_{d,\mathrm{app}}$ for each probe was determined by fitting the protein titration plots to the Hill equation (26). The amount of AMT1 protein active for DNA binding was determined as described previously (17), and the AMT1 protein concentrations indicated in the protein titration plots refer to the amount of AMT1 used in the assay that was active for DNA binding.

For the determination of relative affinity comparisons using modified nucleosides, the following oligonucleotides were produced: wt coding (5′-AGCTAATTTGGCTGAC-3′), wt noncoding (5′-TTAAGTCAGCCAAATT-3′), C-mut coding (5′-AGCTAACTTGGCTGAC-3′), inosine noncoding (5′-TTAAGTCAGCCAAITT-3′), and 3-nitropyrrole (3NP) noncoding [5′-TTAAGTCAGCCAA(3NP)TT-3′] (a gift of Ruthann Nichols). Equal concentrations of the appropriate oligonucleotide pairs were annealed, and the termini were ^{32}P labeled by using the Klenow fragment of DNA polymerase I and [α-^{32}P]dATP (3). The final concentration of each labeled probe was determined spectrophotometrically. Electrophoretic mobility shift assays were performed as described above, and the amounts of probes and proteins used are indicated in the figure legends. The amounts of bound and free species were quantitated as described above.

Missing-nucleoside analysis. Digestion of the plasmid pAMNE with *Hin*dIII revealed the 5′ end of the coding strand for labeling with ^{32}P, and *Eco*RI digestion revealed the 5′ end of the noncoding strand. In all cases in which the oligonucleotides PCR-ABS-1 and PCR-ABS-2 were used to obtain mutant *AMT1* promoter plasmids, *Bam*HI digestion revealed the 5′ end of the coding strand for labeling and *Eco*RI digestion exposed the 5′ end of the noncoding strand for labeling. After phenol-chloroform extraction and ethanol precipitation of the digests, the DNA was subjected to treatment with calf intestinal alkaline phosphatase. The dephosphorylated DNA was labeled on either the coding strand or the noncoding strand by using T4 polynucleotide kinase and [γ-^{32}P]ATP (3). The ^{32}P-labeled DNA was phenol-chloroform extracted and ethanol precipitated. To release the single-end-labeled fragments containing the *AMT1* promoter MRE, the labeled DNA was subjected to a second restriction digest using either *Eco*RI (for coding strand-labeled fragments) or *Hin*dIII (for noncoding strand-labeled fragments) (*Bam*HI was used for PCR-ABS-1- and PCR-ABS-2-derived constructs). The digested single-end-labeled DNA was resolved on a 7.5% native polyacrylamide gel, and the labeled fragments were isolated by electrophoretic transfer of the DNA to DEAE paper as described above. The final DNA preparation was resuspended in 5 mM HEPES (pH 7.9)–100 mM NaCl.

Hydroxyl radical treatment of the single-end-labeled probes was carried out essentially as described by Hayes and Tullius (24). Briefly, labeled probes (~100,000 cpm) were subjected to in vitro hydroxyl radical treatment for 2 min at 25°C in a 100-μl reaction mixture containing 5 μM ammonium iron(II) sulfate (Aldrich), 10 μM EDTA, 0.03% hydrogen peroxide, and 2.5 mM sodium ascorbate. The reactions were terminated by the addition of 100 μl of 0.1 M thiourea. The DNA was then ethanol precipitated and resuspended in 1× binding buffer. Between 150,000 and 200,000 cpm of the hydroxyl radical-treated DNA was used in a 20-μl binding reaction mixture having a final concentration of 2 μM AMT1. Binding was allowed to proceed as described above, and the bound and free DNA species were resolved and isolated as described above by using DEAE paper. Approximately 10,000 to 20,000 cpm of each purified sample was loaded onto an 8% polyacrylamide–8 M urea gel and subjected to electrophoresis at 35 W of constant power to resolve its hydroxyl radical cleavage pattern. Chemical sequencing reaction mixtures for each probe were prepared as previously described (6) and electrophoretically resolved with these samples. The dried gel was analyzed by using the PhosphorImager and software described above.

Ethylation interference assays. Preparation of single-end-labeled probes from the plasmid pAMNE was carried out as described above for the missing-nucleoside experiments. Approximately 500,000 cpm of each probe was subjected to ethylation essentially as described previously (36). DNA probes were resuspended in 100 μl of 50 mM sodium cacodylate (pH 8.0) and mixed with an equal volume of *N*-ethylnitrosourea-saturated ethanol. The reaction was allowed to proceed for 1 h at 50°C, and the ethylated probes were precipitated by the addition of 20 μl of 3 M sodium acetate (pH 5.3) and 550 μl of ethanol. The DNA was washed twice with 70% ethanol and resuspended in 10 μl of 1× binding buffer. Half of each ethylated probe was used in a gel mobility shift assay as described above, with a final AMT1 concentration of 2 μM. Bound and free DNA species were resolved and purified as mentioned above with the exception that the Schleicher & Schuell formamide high-salt buffer was used to elute the DNA from the DEAE paper. After ethanol precipitation of the eluted DNA, each sample was resuspended in 43 μl of 20 mM sodium acetate (pH 5.3) containing 2 mM EDTA, and 7 μl of 2 M NaOH was added to each reaction mixture before the mixtures were placed at 90°C for 30 min. Each probe sample was precipitated with an ethanol-butanol mixture (300 μl of 70% ethanol–600 μl of *n*-butanol). The resulting pellets were resuspended in 100 μl of 1% SDS and reprecipitated with the ethanol-butanol mixture. The final pellets were resuspended in 10 μl of formamide loading buffer (95% formamide, 20 mM EDTA, 0.05% bromophenol blue, 0.05% xylene cyanol). Approximately 6,000 cpm of each sample was loaded onto an 8% polyacrylamide–8 M urea gel and subjected to electrophoresis at 35 W of constant power. Chemical sequencing of the labeled probes was carried out as before, and the sequencing reaction mixtures were resolved alongside the ethylation interference samples. The gel was dried and quantitated by using the PhosphorImager and software described above.

Analysis of wild-type and mutant *AMT1-lacZ* gene expression in vivo. The *C. glabrata ura3*$^-$ strain Q was transformed with plasmids pKTP-8G, pKTP-8A, pKTP-8T, and pKTP-8C by use of the protocol of Ito et al. (31) and plated onto SC-ura agar plates. Liquid cultures of single-colony purified transformants were grown to mid-logarithmic phase (optical density at 650 nm = 1.0 to 2.0) in SC-ura medium at 30°C, and AMT1-dependent transcription was induced by the addition of 100 μM $CuSO_4$ (final concentration) to the medium. At the time points indicated in the figure legends, 3.0-ml aliquots of each culture were removed and briefly spun in two microcentrifuge tubes and the cell pellets were snap-frozen in a dry ice-isopropanol bath. The cell pellets from each time point were kept frozen at −80°C until total RNA was extracted by the hot phenol method described previously (33). RNAs were quantitated spectrophotometrically, and 20 μg of RNA from each time point per sample was used in the RNase protection protocol described below to determine *AMT1-lacZ* and *URA3* mRNA levels.

^{32}P-labeled antisense *AMT1* and *URA3* RNAs were produced from *Bam*HI-cleaved pAIRP2 and pURP, respectively, by using T7 RNA polymerase and [α-^{32}P]UTP in an in vitro transcription protocol (3). The labeled probes were purified on a 6% polyacrylamide–8 M urea gel and eluted at 37°C for 2 h with a solution containing 2 M ammonium acetate, 1% SDS, and 200 μg of glycogen per ml. The RNA probes were ethanol precipitated and resuspended in 50 μl of diethyl pyrocarbonate (DEPC)-treated water. Approximately 1,000,000 cpm of each probe was used in the RNase protection protocol described by Saccomanno et al. (39), with the following modifications. A 20-μg portion of total RNA from each time point was hybridized with approximately 1,000,000 cpm each of the *AMT1* probe and the *URA3* probe for 15 h at 55°C in a 30-μl reaction mixture in 1× hybridization buffer (40 mM PIPES [piperazine-*N*,*N*′-bis(2-ethanesulfonic acid); pH 6.4], 1 mM EDTA, 400 mM NaCl, 50% formamide). Subsequent to hybridization, 250 μl of RNase digestion buffer (50 mM sodium acetate [pH 4.4], 400 mM NaCl, 10 mM EDTA) containing 40 U of RNase T2 (Bethesda Research Laboratories, Grand Island, N.Y.) per ml was added and the reaction mixtures were kept at 30°C for 90 min. The RNA was precipitated at −20°C for 30 min with the addition of 265 μl of 4.0 M guanidine thiocyanate, 530 μl of isopropanol, and 2 μl of 10-mg/ml tRNA. RNA pellets were washed twice with 70% ethanol and resuspended in 10 μl of formamide loading buffer. Four microliters of each sample was loaded per lane on a 6% polyacrylamide–8 M urea gel and subjected to electrophoresis at 35 W of constant power. Gels were dried, and the radioactive bands were quantitated by the methods described above.

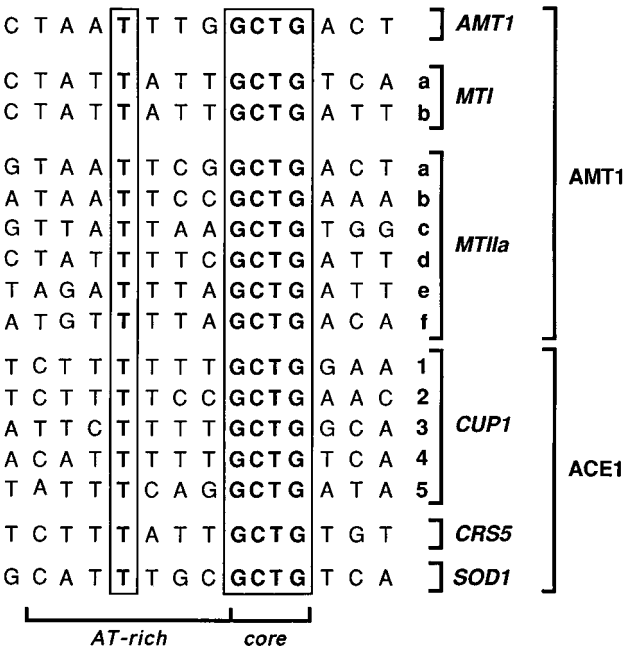

FIG. 1. Comparison of AMT1 and ACE1 binding sites. The regions flanking all of the known ACE1 and AMT1 MREs, from *S. cerevisiae* and *C. glabrata*, are shown. Perfectly conserved residues are boxed. The genes in which the MREs are found are indicated directly to the right of the table, and the corresponding metalloregulatory transcription factor that utilizes the MRE is indicated at the far right side of the table (13, 16, 21, 30, 49).

RESULTS

High-resolution mapping of the AMT1-MRE interactions. Several studies with both yeast cells and mammals have demonstrated that potent metal-responsive transcription requires the presence of multiple MREs in the promoters of target genes. We previously demonstrated that the *C. glabrata AMT1* gene, however, is rapidly transcriptionally induced 15- to 20-fold via CuAMT1 and a single MRE. To begin to understand the mechanisms which underlie this rapid response and to understand the precise interactions of CuMRTFs with DNA, we carried out a detailed investigation of the interactions between CuAMT1 and the *AMT1* MRE. We first conducted a sequence comparison between all known MREs found in target gene promoters which respond to either CuACE1 in *S. cerevisiae* or CuAMT1 in *C. glabrata* to guide us in these studies (Fig. 1). This comparison demonstrated that for the 16 identified sites found in ACE1- or AMT1-responsive promoters, two prominent features emerged. First, although each binding site spans roughly 15 nucleotides, only five positions are perfectly conserved: the GCTG core element and a T located 4 nucleotides upstream of the first G in the GCTG core. Secondly, upstream of each core element a series of at least four consecutive A or T residues is invariably found.

To investigate the details of the molecular interactions between AMT1 and the *AMT1* promoter MRE, full-length AMT1 protein was expressed in *E. coli* and purified (Fig. 2). The purified full-length AMT1 protein has an aberrant electrophoretic mobility during SDS-PAGE which for other proteins has been attributed to high local concentrations of basic residues (27, 41). Amino acid analysis and amino-terminal sequencing of the purified protein established that the preparations were greater than 98% homogeneous and were used to determine the precise protein concentration. DNA electrophoretic mobility shift assays demonstrated that the CuAMT1 protein preparations were fully metallated because of the lack of stimulation of DNA binding by exogenous Cu. Our previous experiments using DNase I footprinting established a region of the *AMT1* promoter encompassing the MRE at relatively low resolution because of the resistance of AT-rich DNA sequences to cleavage by DNase I (7). For example, the initial DNase I footprinting studies could not determine if AMT1 contacted the stretch of 16 adenosine residues upstream of the MRE consensus sequence because of a complete lack of cleavage in this region. To precisely map the boundaries of the AMT1 MRE, and to determine which nucleotide positions make energetically favorable contributions to AMT1 DNA binding, high-resolution mapping studies using hydroxyl radical cleavage-based missing-nucleoside analysis were conducted (24). The results of the missing-nucleoside experiments revealed that a distribution of residues from A−187 to A−197 on the coding strand is critical for AMT1-MRE interactions (Fig. 3A). On the noncoding strand a bipartite distribution of nucleosides critical for AMT1 DNA binding, composed of residues A−185 to C−191 and A−193 to G−199, was observed. Quantitation of the relative effects of these residues, using the PhosphorImager and software described above, revealed the relative importance of each nucleoside position in the MRE for AMT1 binding (Fig. 3B). It should be noted that the cleavage at position −181 in the coding strand was not observed in the pool of free probe in other experiments and therefore does not represent a nucleotide position critical for AMT1-DNA interactions. The missing-nucleoside analysis therefore defined the AMT1 binding site on the *AMT1* promoter as consisting of 15 nucleotides from positions T−185 to C−199 on the coding DNA strand.

Our previous methylation interference studies have implicated the minor groove of the region from A−193 to A−195 as being important for AMT1-DNA interactions (52). Interestingly, the missing nucleoside analysis identified noncoding strand residues A−193 to G−199 as the primary contacts made in the AT-rich half of the *AMT1* promoter MRE. These data, taken together, indicate that some of the critical contacts made on the noncoding strand are made in the minor groove. Furthermore, additional experiments (see below) demonstrate that A−195 plays a critical role in AMT1-DNA interactions in this region, and this correlates well with its absolute conservation in all known yeast MREs.

The results of the missing-nucleoside experiments cannot distinguish between interactions with the nucleotide bases and interactions with the phosphate backbone, since a missing nucleoside would generate a gap in DNA that would allow rotation around the opposite strand, possibly leading to the dis-

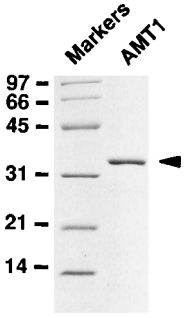

FIG. 2. SDS-PAGE of the purified full-length AMT1 protein. A 2-μg portion of purified AMT1 was analyzed on an SDS–12% polyacrylamide gel stained with Coomassie blue. Purified AMT1 is indicated by the arrowhead. Polypeptide size markers are shown on the left (in kilodaltons).

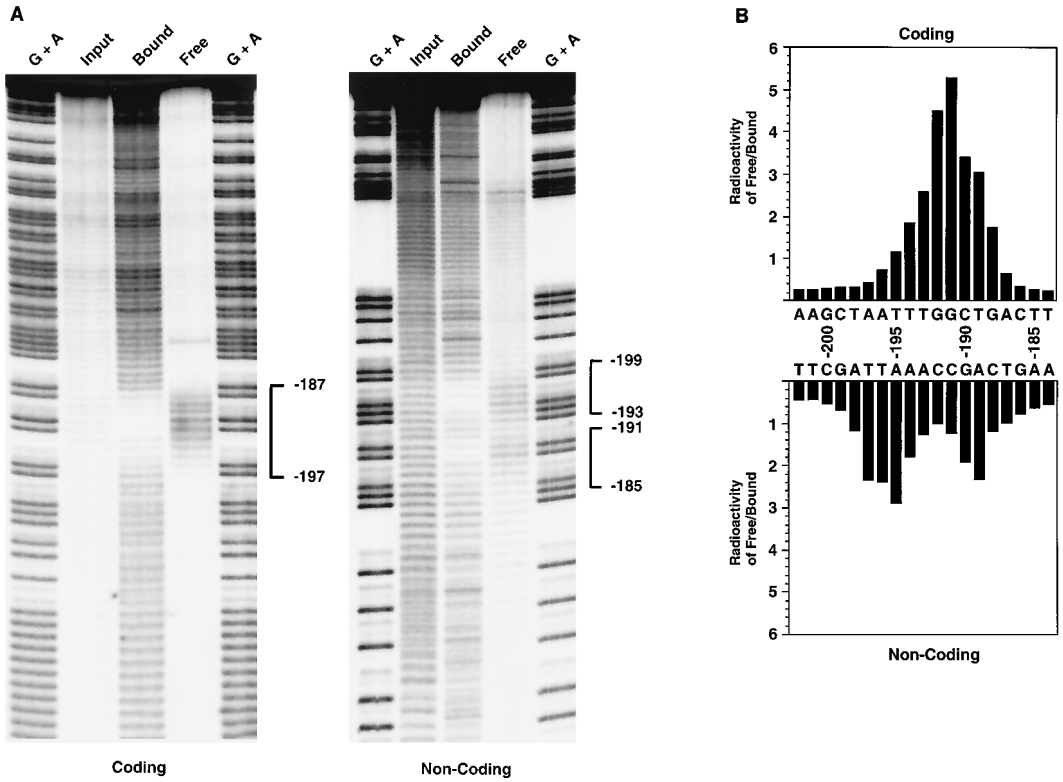

FIG. 3. Missing-nucleoside experiments for the wild-type *AMT1* promoter. (A) The hydroxyl radical cleavage patterns of coding- and noncoding-strand residues critical for AMT1 binding. Lanes: G + A, chemical sequencing reactions of the coding- and noncoding-strand probes; Input, hydroxyl radical-treated DNA that was used in the DNA binding assay with AMT1; Bound, hydroxyl radical-treated DNA that was bound by AMT1; Free, hydroxyl radical-treated DNA that was unable to be bound by AMT1. Critical residues for AMT1 binding are indicated on the right of each gel. (B) Quantitative representation of the data derived from PhosphorImager analysis of the gels in panel A encompassing nucleosides T−184 through A−202.

ruption of the stability of protein-phosphate backbone contacts made around the position of the gap. To more thoroughly characterize the nature of AMT1-MRE interactions, phosphate backbone interactions important for AMT1 DNA binding were mapped by ethylation interference assays using *N*-ethylnitrosourea as previously described (36). As shown in Fig. 4A, ethylation of the 3′ phosphate on AMT1 promoter coding-strand residues G−188, G−191, G−192, and T−193 and noncoding-strand residues G−186, T−187, A−189, G−190, A−194, and A−195 prevented or severely reduced the formation of a stable AMT1-DNA complex. Quantitation of the relative effect of each of the ethylation events demonstrated that the critical phosphate backbone interactions were completely encompassed within the AMT1 binding site as determined by the missing-nucleoside analysis (Fig. 4B). Furthermore, the critical contacts that are made at the 3′ phosphates of noncoding-strand residues A−194 and A−195 effectively flank residue A−195, which is the perfectly conserved adenosine residue within the AT-rich half of the MRE.

Using purified full-length CuAMT1 in quantitative electrophoretic mobility shift assays, we determined the dissociation constant for the complex between AMT1 and the *AMT1* promoter. As shown in Fig. 5, AMT1 binds to the wild-type *AMT1* promoter MRE with a $K_{d,app}$ of 3×10^{-10} M, which is not altered by the presence or absence of the unusual stretch of 16 adenosine residues located 10 nucleotides upstream of the MRE. Therefore, AMT1 binds to the *AMT1* promoter MRE with very high affinity. Circular permutation electrophoretic mobility shift experiments did not reveal a large amount of DNA distortion by bound AMT1 (data not shown).

The data from previous methylation interference studies (52), the missing-nucleoside experiments, and the ethylation interference assays described above have been compiled in a computer graphics simulation of the *AMT1* promoter MRE (Fig. 6). The residues indicated in Fig. 6 comprise all of the nucleosides determined to be critical for AMT1-DNA interactions by the missing-nucleoside experiments. In this three-dimensional depiction of the *AMT1* promoter MRE, the location of AMT1 on DNA becomes apparent. The compiled data are consistent with monomeric AMT1 interacting with one face of the DNA double helix at adjacent major and minor grooves, with critical phosphate backbone contacts being made at sites in both grooves as well as at sites along the bridging phosphate backbone that AMT1 must traverse to make these adjacent contacts.

A contact in the MRE minor groove is critical for DNA binding. As summarized in Fig. 6, the binding of AMT1 to the *AMT1* MRE involves contacts in the minor groove at the conserved T · A base pair positioned 4 nucleotides upstream of the GCTG core element. The A residue on the noncoding strand opposite this T−195 is flanked by phosphates which make critical contributions to AMT1 binding. To ascertain the importance of this minor groove contact for AMT1 binding in vitro and the requirement, if any, for the conservation of an A residue at this position, *AMT1* promoter fragments having each of the four possible base pairs at this position were ^{32}P labeled and used in quantitative electrophoretic mobility shift assays (Fig. 7). PhosphorImager analysis of the binding reaction mixtures demonstrated that mutagenesis of the conserved T at position −195 on the coding strand to A, C, or G resulted

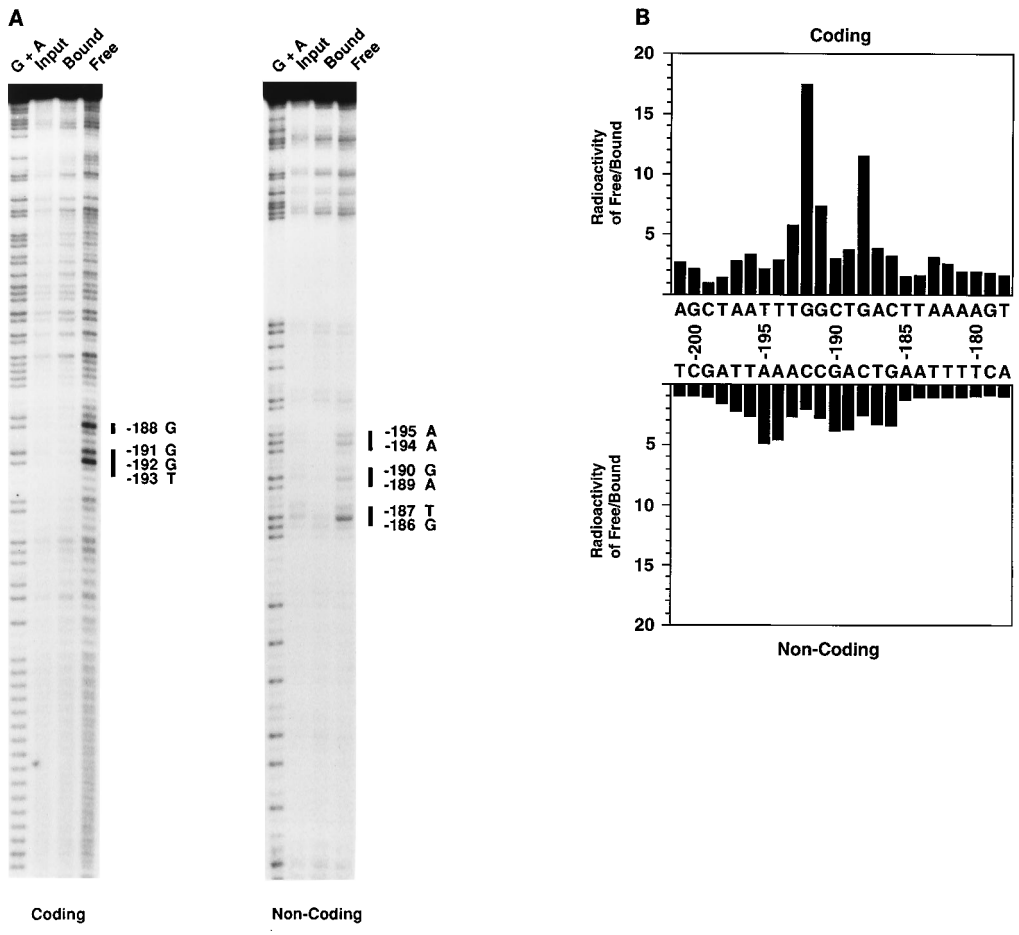

FIG. 4. Ethylation interference assay of AMT1 bound to the *AMT1* MRE. (A) Lanes: G+A, chemical sequencing reactions of the coding- and noncoding-strand probes; Input, ethylated DNA that was used in the DNA binding assay with AMT1; Bound, ethylated DNA that was bound by AMT1; Free, ethylated DNA that was unable to be bound by AMT1. Residues that interfere with AMT1 binding when ethylated are indicated on the right of each gel. (B) Quantitative representation of the data shown in panel A for residues T−178 through A−201.

in a 20, 80, or 97% reduction in DNA binding by AMT1, respectively. Furthermore, replacement of the T · A base pair at this position by a C · I (where I represents inosine) base pair in a synthetic oligonucleotide resulted in wild-type AMT1 binding affinity (Fig. 7, lanes C:I). Given that a C · I base pair is chemically identical to an A · T base pair in the minor groove but distinct from A · T in the major groove, these results strongly support the prediction that AMT1 interacts only in the minor groove of the perfectly conserved T · A base pair. The introduction of a guanine exocyclic amine in the minor groove by placement of a G · C or C · G base pair at this position, much like the methylation of the A residue at the N-3 position, would likely present steric hindrance to minor groove access and perhaps interfere with access to the phosphate backbone. Moreover, substitution of 3NP, which offers no hydrogen bond acceptors in either the major groove or the minor groove, for the A on the noncoding strand at this position resulted in only a twofold reduction in AMT1 DNA binding affinity (Fig. 7, lanes T:3NP). This observation may suggest that AMT1 interacts with the N-3 atom of A in the minor groove but that this is not a major stabilizing interaction or that 3NP causes a subtle distortion of the minor groove structure in this region that affects the ability of AMT1 to interact with adjacent bases.

***AMT1* transcription requires the conserved minor groove interaction.** The in vitro DNA binding studies described above establish the important contribution of the minor groove interaction at the A · T base pair at position −195. To test whether this contact is critical for CuAMT1-dependent transcriptional activation from this MRE, the wild type and three mutant derivative promoters were fused to the *E. coli lacZ* gene, as a translational fusion, and introduced into the *ura3*$^{-}$-*AMT1* wild-type *C. glabrata* strain Q (50). Figure 8 shows the results of RNase protection experiments in which steady-state mRNA levels, driven from the wild-type or mutant *AMT1-lacZ* fusion genes and the chromosomal *C. glabrata URA3* gene as an internal control, were assessed as a function of time after exposure to Cu. Consistent with our previous observations, *AMT1-lacZ* mRNA levels driven from the wild-type promoter increased rapidly after Cu administration, with an approximately 13-fold induction after 30 min, whereas the A mutant-*lacZ* mRNA levels were maximally induced less than fourfold. We observed very little, if any, induction of *AMT1-lacZ* mRNA driven from promoters containing either C or G on the coding strand at position −195. Therefore, the induction of *AMT1-lacZ* mRNA from the wild-type and mutant *AMT1* promoters parallels their relative in vitro DNA binding affinities. These data strongly suggest a critical role of the minor groove contact at this position in the *AMT1* MRE and support the theory that the conservation of a T · A base pair minor groove interaction

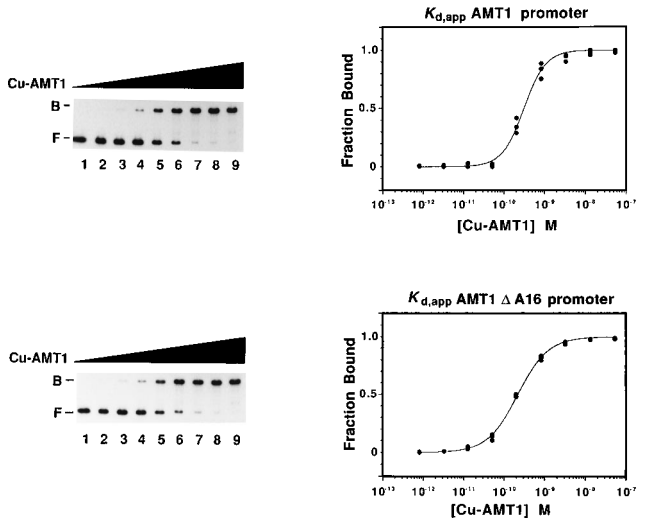

FIG. 5. AMT1 binding site affinity determination. (Top) The left panel is a representative 6% electrophoretic mobility shift gel of the wild-type ^{32}P-labeled *AMT1* promoter fragment titrated with increasing amounts of purified AMT1. AMT1 concentrations used were 8.0×10^{-13} M, 3.2×10^{-12} M, 1.3×10^{-11} M, 5.2×10^{-11} M, 2.1×10^{-10} M, 8.3×10^{-10} M, 3.3×10^{-9} M, 1.3×10^{-8} M, and 5.4×10^{-8} M for lanes 1 to 9, respectively. The right panel represents the protein titration plots derived from three replicate titration experiments. (Bottom) The left panel is a representative 6% electrophoretic mobility shift gel of the ^{32}P-labeled *AMT1* promoter fragment lacking the 16-adenosine (A16) tract titrated with increasing amounts of purified AMT1. Concentrations of AMT1 used were the same as those used for the top left panel. The right panel represents the protein titration plot derived from three replicate titration experiments.

at position −195 is optimal for Cu-responsive transcriptional activation by CuMRTFs.

A conserved minor groove binding motif in AMT1. The use of both major groove and minor groove DNA contacts for AMT1 DNA binding is relatively rare among sequence-specific DNA-binding proteins. However, a number of proteins of both prokaryotic and eukaryotic origin are now known to utilize both types of contacts. A minor groove binding motif which harbors the critical core sequence glycine-arginine-proline (GRP) is known to interact with A · T base pairs in the minor groove of AT-rich DNA (20, 47). Recent studies have demonstrated that a peptide corresponding to the GRP domain of the high mobility group I protein (HMG-I) selectively binds to the minor groove within the sequence 5′-AATT-3′; however, the same peptide in which lysine was substituted for arginine failed to bind to this sequence (20). Figure 9A demonstrates that this motif is conserved in both known CuMRTFs, AMT1 and ACE1, as well as in the MAC1 protein, a nuclear factor important for the expression of the *FRE1* gene encoding an iron/copper reductase (32). To test the possibility that this region of AMT1 plays an important role in MRE binding, the arginine at position 38 was altered to lysine (R38K) by site-directed mutagenesis of the *AMT1* gene and the protein was expressed in and purified from *E. coli*. Comparison of the wild-type AMT1 protein with the R38K mutant protein in quantitative electrophoretic mobility shift assays revealed that R38K had at least a fivefold reduction in DNA binding affinity for the MRE (Fig. 9B). These results suggest that the GRP motif in AMT1 plays an important role in DNA binding and may specifically interact with the conserved T · A base pair in the MRE minor groove; however, the question of whether

FIG. 6. Computer graphics image of the *AMT1* promoter MRE compiling the data from missing-nucleoside experiments, ethylation interference assays, and methylation interference assays (49). Methylated residues that interfere with AMT1 binding are shown in white. Ethylated backbone phosphates that interfere with AMT1 binding are indicated in yellow. Coding-strand conserved residues are indicated in red, and noncoding-strand conserved residues are indicated in blue. This image was produced by using Biopolymer and Insight II software on an Indigo II Silicon Graphics workstation.

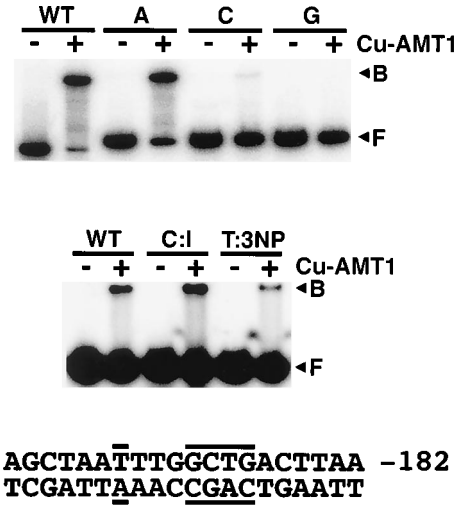

FIG. 7. Binding of AMT1 to the mutant *AMT1* promoter MREs. (Top) Six percent mobility shift gel of AMT1 binding to the wild-type (WT) base (T) and to A, C, and G base substitutions at position −195 of the *AMT1* promoter. In each case, the concentration of the ^{32}P-labeled DNA probe was 3.3 μM and the concentration of purified AMT1 used was 20 nM. (Middle) Six percent mobility shift gel of AMT1 binding to probes having a T · A (wild-type) base pair, a C · I (where I represents inosine) base pair (C:I), or a T · 3NP base pair (T:3NP) at position −195. (Bottom) Sequence of the T · A 20-bp oligonucleotide binding site that was used in the middle gel; the C · I and T · 3NP binding sites had the same composition except for the base change at position −195.

there is a direct interaction between the R-38 residue and the minor groove must await structural information on the AMT1-DNA complex. The change from arginine to lysine has conserved the basic nature of this residue and therefore has not changed the overall charge of the AMT1 DNA binding domain. Furthermore, on the basis of co-crystal structures of other proteins which utilize the GRP motif, such as *E. coli* Hin recombinase and *Drosophila melanogaster* prd, it is clear that other amino acid residues within the GRP domain make important contributions to minor groove binding.

Since the *AMT1* gene both is autoactivated and serves to activate transcription of the family of *C. glabrata* MT genes, we tested the functional consequences of the AMT1 R38K mutation for the ability of *C. glabrata* cells to mount a copper detoxification response. To test the biological consequences of the R38K mutation in the AMT1 GRP motif, the *AMT1* wild-type and *AMT1 R38K* alleles were independently integrated at the *C. glabrata ura3*$^-$ locus, in single copies, in a strain harboring an insertionally inactivated *AMT1* allele (*amt1-1*) and tested for resistance to increasing concentrations of Cu. Western blot

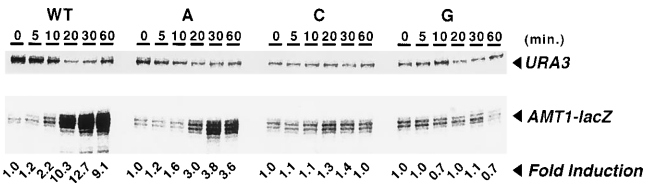

FIG. 8. RNase protection analysis of transcriptional induction of the wild-type *AMT1* promoter (WT) and *AMT1* promoter mutants with mutations (to A, C, or G) at position −195. *URA3* and *AMT1-lacZ* mRNA levels were analyzed in a time course of induction with 100 μM $CuSO_4$ by using the RNase protection protocol described in Materials and Methods. Quantitation was carried out with a PhosphorImager, and in each case the *AMT1-lacZ* mRNA level was normalized to the respective *URA3* mRNA level. The fold induction for each fusion gene is indicated at the bottom of the figure.

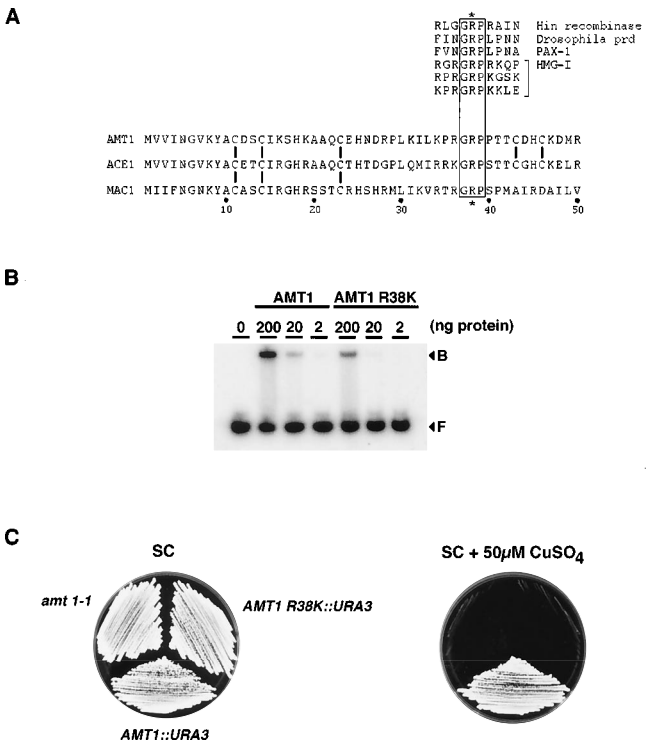

FIG. 9. Mutational analysis of a potential AMT1 minor groove binding domain. (A) Amino acid sequence alignment of the amino-terminal 50 amino acids of the AMT1 (51), ACE1 (43), and MAC1 (32) proteins with the conserved GRP motif boxed. The conserved cysteine residues are indicated with bold lines, and the critical arginine-38 residue is indicated by the asterisk. Also included are the 10 amino acid peptides that encompass GRP motifs in the *E. coli* Hin recombinase (53), *Drosophila* prd (8), mouse Pax-1 (14), and human HMG-I proteins (35). (B) Comparison of the relative DNA binding affinities of the wild-type AMT1 and AMT1 R38K proteins. Electrophoretic mobility shift analysis was performed with the indicated amounts of wild-type AMT1 or AMT1 R38K protein purified from *E. coli* and the T · A (wild type) probe used for Fig. 8. Bound (B) and free (F) species are indicated, and the concentration of probe in each case was 3.3 μM. (C) The copper resistance phenotypes for the *amt1-1*, *AMT1*::*URA3*, and *AMT1 R38K*::*URA3* strains grown on synthetic complete medium supplemented with 50 μM $CuSO_4$.

(immunoblot) analysis demonstrated that the basal steady-state levels of the wild-type and AMT1 R38K proteins were comparable (data not shown). As previously observed (52), Fig. 9C demonstrates that *C. glabrata* cells harboring the wild-type *AMT1* gene were resistant to Cu; however, cells containing both the *AMT1 R38K* and *amt1-1* alleles were defective in mounting a response to very low levels of Cu. These results demonstrate that the R-38 residue, which is known to play an important role in minor groove recognition in proteins with the GRP motif, is important for high-affinity binding of AMT1 to the MRE, for activation of *AMT1* MRE-dependent transcription, and for the ability of *C. glabrata* cells to mount a normal detoxification response to elevated environmental Cu concentrations.

DISCUSSION

The CuMRTFs AMT1 and ACE1 are members of a unique class of transcriptional activator proteins which utilize a ligand-activated DNA binding domain, through the formation of a polynuclear Cu cluster, to sense and transcriptionally respond to elevations in Cu levels. The binding of CuMRTF proteins delivers a potent transcriptional activation domain to the pro-

moters of Cu-responsive genes to activate gene expression. Therefore, the rapidity and stability with which CuMRTFs bind to MRE sequences are critical rate-limiting factors in target gene activation in the face of potentially toxic Cu levels. Since the CuMRTFs are structurally distinct from other known classes of DNA-binding proteins, determination of the mechanisms by which CuMRTFs interact with MRE elements, and the biological importance of these interactions, is important in formulating a comprehensive understanding of metal-responsive cell signalling and Cu homeostasis.

Taken together, the results of missing-nucleoside analysis, ethylation interference, methylation interference, and site-directed mutagenesis demonstrate that the AMT1 protein binds to MRE sequences via critical contacts in both the major and minor grooves. The observation that AMT1 binds to both MT gene MREs and the single *AMT1* MRE (32a) as a monomer may suggest that two subdomains exist in the AMT1 Cu-activated DNA binding domain to engage in these contacts with the asymmetric MRE binding site. The two subdomains could represent two independent Cu clusters with distinct DNA binding specificities or a single Cu cluster that simply has two DNA interaction domains present in its overall structure. Alternatively, since it has been observed that truncated versions of both AMT1 and ACE1 purified from *E. coli* contain a single Zn atom (46), it is possible that Zn coordination forms or assists in the formation of one of the putative subdomains. The biological role of a bound Zn atom in CuMRTF function has not yet been established.

Although the AMT1 and ACE1 proteins have 50% amino acid sequence identity in the first 122 amino acids encompassing the copper coordination-DNA binding domain, there are subtle differences in the contacts that the proteins utilize in interacting with their respective MREs. A truncated ACE1 protein was shown to interact with additional upstream major groove sites 5′ to the AT-rich portion in the left arm of *CUP1* upstream activation sequence C (UAS_C). Our previous methylation interference studies (52), as well as the results of the missing-nucleoside analysis and ethylation interference assays presented here, clearly show that the full-length AMT1 protein does not make additional upstream major groove contacts with the *AMT1* MRE. This point is further supported by the observation that there are no absolutely conserved residues among the known yeast MREs in the region of the upstream major groove contacts made by the truncated ACE1 protein. Additionally, minor groove methylation of the N-3 of adenine across from the conserved T in the GCTG core was shown to interfere with the binding of the truncated ACE1 protein to the UAS_C (15). Again, the experiments shown here and our previous studies using the full-length AMT1 protein have not detected AMT1-DNA interactions on the minor groove face of the GCTG core.

Three lines of evidence support the possibility that ACE1 and AMT1 make direct protein-nucleotide edge contacts at the conserved T · A base pair at position −195. First, this base pair is absolutely conserved in all known yeast MREs, even though the minor groove environments for T · A and A · T base pairs are essentially identical. Second, a transversion mutation that generates an A · T base pair results in a 20% reduction in DNA binding in vitro and a 70% reduction in transcription from a promoter harboring this point mutation in vivo. This is particularly strong evidence in light of the fact that a transversion from T · A to A · T would not affect the phosphate backbone contacts made on either side of noncoding-strand position −195. Finally, replacement of the adenine in the T · A base pair with 3NP, which effectively removes the N-3 of adenine from potential contacts with AMT1, results in a 43% reduction in DNA binding in vitro, although we cannot preclude subtle structural changes that the 3NP may impose on double-stranded DNA as the cause of the decreased binding affinity.

One possible explanation for the differences between the effect that the base substitutions have on DNA binding in vitro and the more dramatic effects on transcription in vivo is that DNA binding could be followed by a distortion in DNA that is necessary for transcription. This phenomenon has been elegantly described for the metalloregulation of the *E. coli* Mer operon by the MerR protein (1). In this view, the mutant MREs would be able to be bound by AMT1 with weakened affinity in vitro but might be incapable of being distorted properly, resulting in the more dramatic effects seen in vivo. It should be noted that many of the paired-domain proteins that use the GRP motif distort DNA (12, 47). We have therefore tested the possibility that AMT1 distorts DNA upon binding to the *AMT1* promoter MRE by circular permutation analysis (data not shown). By this analysis, we were unable to detect significant DNA distortion upon AMT1 binding. Therefore, the differences seen in vivo may represent differences between the binding of AMT1 to naked DNA and binding to the DNA and its associated proteins found in the cell nucleus, which may be influenced by other, as yet unidentified auxiliary factors.

To date, the phenotype of mice bearing a homozygous *undulated* mutation represents the clearest example of the biological ramifications of mutations within a GRP motif in higher eukaryotic organisms. A mouse homozygous for the *undulated* mutation exhibits severe vertebral malformations that are the consequence of a point mutation within the paired-box-containing gene *Pax-1* (5). The point mutation that results in the *undulated* phenotype converts the conserved glycine within the GRP motif to serine in the Pax-1 paired domain. Other missense mutations that map to the region of the GRP within the paired domains of other Pax proteins include PAX-3(BU47), in which a conserved Asn adjacent to the GRP is changed to His, and PAX(BU26), which has the conserved Pro residue in the GRP changed to Leu (4, 28). The X-ray co-crystal structure between the *Drosophila* prd protein and its cognate DNA binding site has provided critical insight into the interactions made by the paired-domain GRP motif with DNA and has consequently furthered our understanding of the implications that each of the aforementioned Pax developmental mutations has for the ability of the mutant protein to interact with DNA (47). The GRP motif of the *Drosophila* prd protein resides within a type II β turn that lies deep within the minor groove of its cognate DNA binding site (47). On the basis of the X-ray co-crystal structure, each of the previously described Pax developmental mutations would likely result in disruption of critical protein-DNA contacts and/or impose steric constraints preventing the ability of the type II β turn to enter deep into the minor groove, ultimately affecting DNA binding by the mutant proteins.

A series of nuclear magnetic resonance studies investigating the interactions of peptides, which contain the GRP domain, from the HMG-I protein have shown that the Arg at the center of this motif is absolutely critical for sequence-specific DNA interactions within the minor groove (20). When the Arg was changed to Lys, sequence-specific DNA interactions were lost. Furthermore, the nuclear magnetic resonance results confirmed that the GRP motif resides deep within the minor groove. With this information, we investigated the effect of an Arg-to-Lys substitution within the AMT1 GRP motif on DNA binding both in vitro and in vivo in the context of the Cu resistance afforded by the mutant protein. In a manner similar to that observed for the Arg-to-Lys substitution in the HMG-I peptides, the DNA binding affinity of the AMT1 R38K protein

was reduced by nearly 80%. The more severe biological consequences of this mutation (Fig. 9C) are likely the result of four factors. First, at its basal level the AMT1 R38K protein that is made constitutively has a weakened affinity for DNA, which would reduce its capacity to autoregulate its own transcription during Cu exposure. Secondly, the diminished autoactivation provided by AMT1 R38K would result in less AMT1 R38K protein being made and consequently reduced Cu resistance as was shown for the *AMT1(m)::URA3* allele (52). Thirdly, the small amount of AMT1 R38K that is ultimately made through autoregulation would also have a weakened affinity for the MREs found in each of the MT gene promoters, resulting in greatly reduced MT production. Finally, since AMT1 has been shown to be either directly or indirectly involved in supporting the steady-state levels of mRNA from the *MT-1* and *MT-II* genes (49), it is possible that the AMT1 R38K protein would also be defective in this role, making cells acutely sensitive to instantaneous Cu exposure. Therefore, the *AMT1 R38K* mutation, like *undulated* in mice, has severe biological consequences with respect to the development of an appropriate response to a stimulus.

This report provides the first evidence that a known DNA binding motif is utilized by yeast CuMRTFs. The observation that many GRP-utilizing proteins from higher eukaryotes have two distinct domains that interact with adjacent major and minor grooves suggests that the GRP domain may be a modular entity, and as with *E. coli* Hin recombinase, yeast CuMRTFs may be evolutionary precursors to the higher eukaryotic transcription factors that utilize the GRP motif. Consistent with the hypothesis that the GRP domain is part of a modular entity, Ashar et al. have recently discovered human lipomas having chromosome 12 rearrangements that fuse the three amino-terminal human HMGI-C GRP domains with transcriptional regulatory domains (2). The normally inactive HMGI-C acidic domain is replaced by a functional transcriptional activation domain in these chromosomal rearrangements. This mutation may result in a gain-of-function for the fusion protein with concomitant deregulation of the HMGI-C downstream target genes, presumably leading to lipoma formation. The GRP motif found in both AMT1 and ACE1 may constitute a functionally distinct subdomain within the DNA binding domain that is used to interact with the AT-rich minor groove. Our ability to draw upon the HMG-I peptide nuclear magnetic resonance data and the X-ray co-crystal structure of either *E. coli* Hin recombinase or *Drosophila* prd to assign a direct interaction between the AMT1 R-38 residue and a specific nucleotide or phosphate in the MRE is severely limited by the lack of a consensus for the GRP interactions. For example, the guanidinium protons of Arg-6 in a GRP of HMG-I make hydrogen bond contacts with N-3 of an adenosine residue (20), whereas Arg-16 in the *Drosophila* prd GRP makes both a water-mediated hydrogen bond to the O-2 of a thymidine residue and van der Waals interactions with the phosphate backbone (47). The data presented here provide strong evidence supporting the use of the GRP motif by the AMT1 protein in its interactions with the AT-rich minor groove of MREs. However, given the lack of a clear consensus for GRP-DNA interactions, the assignment of specific contacts made between the amino acids of the AMT1 protein and the nucleosides within the MRE must await determination of the structure of the AMT1-DNA complex.

ACKNOWLEDGMENTS

We thank David Engelke, Tom Kerppola, Zhiwu Zhu, and Simon Labbé for critically reading the manuscript and for their valuable suggestions. We also thank Zhiwu Zhu for the plasmid pBZ12-A16Δ, Ruthann Nichols for the 3NP-containing oligonucleotide, and Tom Tullius for his helpful discussions regarding the missing-nucleoside experiments.

This work was supported by National Institutes of Health grant GM41840 to D.J.T. and by National Institutes of Health grant M01-RR00042 to the General Clinical Research Center, University of Michigan Medical Center. K.A.K. was supported in part by the Cellular Biotechnology Training Program NIH grant GM08353. D.J.T. is a Burroughs Wellcome Toxicology Scholar.

REFERENCES

1. **Ansari, A. Z., M. L. Chael, and T. V. O'Halloran.** 1992. Allosteric underwinding of DNA is a critical step in positive control of transcription by Hg-MerR. Nature (London) **355:**87–89.
2. **Ashar, H. R., M. Schoenberg Fejzo, A. Tkachenko, X. Zhou, J. A. Fletcher, S. Weremowicz, C. C. Morton, and K. Chada.** 1995. Disruption of the architectural factor HMGI-C: DNA-binding AT hook motifs fused in lipomas to distinct transcriptional regulatory domains. Cell **82:**57–65.
3. **Ausubel, F. M., R. Brent, R. E. Kingston, D. D. Moore, J. G. Seidman, J. A. Smith, and K. Struhl.** 1987. Current protocols in molecular biology. John Wiley & Sons, New York.
4. **Baldwin, C. T., C. F. Hoth, J. A. Amos, E. O. da-Silva, and A. Milunsky.** 1992. An exonic mutation in the *HuP2* paired domain gene causes Waardenburg's syndrome. Nature (London) **355:**637–638.
5. **Balling, R., U. Deutsch, and P. Gruss.** 1988. *undulated*, a mutation affecting the development of the mouse skeleton, has a point mutation in the paired box of Pax 1. Cell **55:**531–535.
6. **Bencini, D. A., G. A. O'Donovan, and J. R. Wild.** 1984. Rapid chemical degradation sequencing. BioTechniques **2:**4.
7. **Bernardi, A., C. Gaillard, and G. Bernardi.** 1975. The specificity of five DNAases as studied by analysis of 5′-terminal doublets. Eur. J. Biochem. **52:**451–457.
8. **Bopp, D., M. Burri, S. Baumbartner, G. Frigerio, and M. Noll.** 1986. Conservation of a large protein domain in the segmentation gene *paired* and in functionally related genes of Drosophila. Cell **47:**1033–1040.
9. **Buchman, C., P. Skroch, W. Dixon, T. D. Tullius, and M. Karin.** 1990. A single amino acid change in CUP2 alters its mode of DNA binding. Mol. Cell. Biol. **10:**4778–4787.
10. **Buchman, C., P. Skroch, J. Welch, S. Fogel, and M. Karin.** 1989. The *CUP2* gene product, regulator of yeast metallothionein expression, is a copper-activated DNA-binding protein. Mol. Cell. Biol. **9:**4091–4095.
11. **Carrì, M. T., F. Galiazzo, M. R. Ciriolo, and G. Rotilio.** 1991. Evidence for co-regulation of Cu,Zn superoxide dismutase and metallothionein gene expression in yeast through transcriptional control by copper via the ACE1 factor. FEBS Lett. **2278:**263–266.
12. **Chalepakis, G., J. Wijnholds, and P. Gruss.** 1994. Pax-3-DNA interaction: flexibility in the DNA binding and induction of DNA conformational changes by paired domains. Nucleic Acids Res. **22:**3131–3137.
13. **Culotta, V. C., W. R. Howard, and X. Liu.** 1994. *CRS5* encodes a metallothionein-like protein in *Saccharomyces cerevisiae*. J. Biol. Chem. **269:**25295–25302.
14. **Deutsch, U., G. R. Dressler, and P. Gruss.** 1988. *Pax 1*, a member of a paired box homologous murine gene family, is expressed in segmented structures during development. Cell **53:**617–625.
15. **Dobi, A., C. T. Dameron, S. Hu, D. Hamer, and D. R. Winge.** 1995. Distinct regions of Cu(I)-ACE1 contact two spatially resolved DNA major groove sites. J. Biol. Chem. **270:**10171–10178.
16. **Evans, C. F., D. R. Engelke, and D. J. Thiele.** 1990. ACE1 transcription factor produced in *Escherichia coli* binds multiple regions within yeast metallothionein upstream activation sequences. Mol. Cell. Biol. **10:**426–429.
17. **Fried, M., and D. M. Crothers.** 1981. Equilibria and kinetics of lac repressor-operator interactions by polyacrylamide gel electrophoresis. Nucleic Acids Res. **9:**6505–6525.
18. **Fürst, P., and D. Hamer.** 1989. Cooperative activation of a eukaryotic transcription factor: interaction between Cu(I) and yeast ACE1 protein. Proc. Natl. Acad. Sci. USA **86:**5267–5271.
19. **Fürst, P., S. Hu, R. Hackett, and D. Hamer.** 1988. Copper activates metallothionein gene transcription by altering the conformation of a specific DNA binding protein. Cell **55:**705–717.
20. **Geierstanger, B. H., B. F. Volkman, W. Kremer, and D. E. Wemmer.** 1994. Short peptide fragments derived from HMG-I/Y proteins bind specifically to the minor groove of DNA. Biochemistry **33:**5347–5355.
21. **Gralla, E. B., D. J. Thiele, P. Silar, and J. S. Valentine.** 1991. ACE1, a copper-dependent transcription factor, activates expression of the yeast copper, zinc superoxide dismutase gene. Proc. Natl. Acad. Sci. USA **88:**8558–8562.
22. **Halliwell, B.** 1994. Free radicals and antioxidants: a personal review. Nutr. Rev. **52:**253–265.
23. **Halliwell, B., and J. M. C. Gutteridge.** 1990. Role of free radicals and catalytic metal ions in human disease: an overview. Methods Enzymol. **186:** 1–85.

24. **Hayes, J. J., and T. D. Tullius.** 1989. The missing nucleoside experiment: a new technique to study recognition of DNA by protein. Biochemistry **28:** 9521–9527.
25. **Heuchel, R., F. Radtke, and W. Schaffner.** 1995. Transcriptional regulation by heavy metals, exemplified at the metallothionein genes, p. 206–240. *In* P. A. Baeuerle (ed.), Inducible gene expression, vol. 1. Birkhäuser, Boston.
26. **Hill, A. V.** 1910. The possible effects of aggregation of the molecules of hæmoglobin on its dissociation curves. J. Physiol. (London) **40:**iv.
27. **Hope, I. A., and K. Struhl.** 1986. Functional dissection of a eukaryotic transcriptional activator protein, GCN4 of yeast. Cell **46:**885–894.
28. **Hoth, C. F., A. Milunsky, N. Lipsky, R. Sheffer, S. K. Clarren, and C. T. Baldwin.** 1993. Mutations in the paired domain of the human PAX3 gene cause Klein-Waardenburg syndrome (WS-III) as well as Waardenburg syndrome type I (WS-I). Am. J. Hum. Genet. **52:**455–462.
29. **Hu, S., P. Fürst, and D. Hamer.** 1990. The DNA and Cu binding function of ACE1 are interdigitated within a single domain. New Biol. **2:**544–555.
30. **Huibregtse, J. M., D. R. Engelke, and D. J. Thiele.** 1989. Copper-induced binding of cellular factors to yeast metallothionein upstream activation sequences. Proc. Natl. Acad. Sci. USA **86:**65–69.
31. **Ito, H., Y. Fukada, K. Murata, and A. Kimura.** 1983. Transformation of intact yeast cells treated with alkali cations. J. Bacteriol. **153:**163–168.
32. **Jungmann, J., H.-A. Reins, J. Lee, A. Romeo, R. Hassett, D. Kosman, and S. Jentsch.** 1993. MAC1, a nuclear regulatory protein related to Cu-dependent transcription factors is involved in Cu/Fe utilization and stress resistance in yeast. EMBO J. **12:**5051–5056.
32a. **Koch, K. A., and D. J. Thiele.** Unpublished data.
33. **Köhrer, K., and H. Domdey.** 1991. Preparation of high molecular weight RNA. Methods Enzymol. **194:**398–405.
34. **Linder, M. C.** 1991. Biochemistry of copper. Plenum Press, New York.
35. **Lund, T., K. H. Dahl, E. Mørk, J. Holtlund, and S. G. Laland.** 1987. The human chromosomal protein HMG I contains two identical palindrome amino acid sequences. Biochem. Biophys. Res. Commun. **146:**725–730.
36. **Majumdar, A., and S. Adhya.** 1989. Effect of ethylation of operator-phosphates on Gal repressor binding. J. Mol. Biol. **208:**217–223.
37. **O'Halloran, T. V.** 1993. Transition metals in control of gene expression. Science **261:**715–725.
38. **Predki, P. F., and B. Sarkar.** 1992. Effect of replacement of "zinc finger" zinc on estrogen receptor DNA interactions. J. Biol. Chem. **267:**5842–5846.
39. **Saccomanno, C. F., M. Bordonaro, J. S. Chen, and J. L. Nordstrom.** 1992. A faster ribonuclease protection assay. BioTechniques **13:**846–850.
40. **Sherman, F., G. R. Fink, and J. B. Hicks.** 1986. Methods in yeast genetics. Cold Spring Harbor Laboratory, Cold Spring Harbor, N.Y.
41. **Sorger, P. K., and H. R. B. Pelham.** 1988. Yeast heat shock factor is an essential DNA-binding protein that exhibits temperature-dependent phosphorylation. Cell **54:**855–864.
42. **Studier, F. W., A. H. Rosenberg, J. J. Dunn, and J. W. Dubendorff.** 1990. Use of T7 RNA polymerase to direct expression of cloned genes. Methods Enzymol. **185:**60–89.
43. **Szczypka, M., and D. J. Thiele.** 1989. A cysteine-rich nuclear protein activates yeast metallothionein gene transcription. Mol. Cell. Biol. **9:**421–429.
44. **Thiele, D. J.** 1988. ACE1 regulates expression of the *Saccharomyces cerevisiae* metallothionein gene. Mol. Cell. Biol. **8:**2745–2752.
45. **Thiele, D. J.** 1992. Metal-regulated transcription in eukaryotes. Nucleic Acids Res. **20:**1183–1191.
46. **Thorvaldsen, J. L., A. K. Sewell, A. M. Tanner, J. M. Peltier, I. J. Pickering, G. N. George, and D. R. Winge.** 1994. Mixed Cu^{+} and Zn^{2+} coordination in the DNA-binding domain of the AMT1 transcription factor from *Candida glabrata*. Biochemistry **33:**9566–9577.
47. **Xu, W., M. A. Rould, S. Jun, C. Desplan, and C. O. Pabo.** 1995. Crystal structure of a paired domain-DNA complex at 2.5 Å resolution reveals structural basis for Pax developmental mutations. Cell **80:**639–650.
48. **Zhang, S. P., G. Zubay, and E. Goldman.** 1991. Low-usage codons in Escherichia coli, yeast, fruit fly and primates. Gene **105:**61–72.
49. **Zhou, P., M. S. Szczypka, T. Sosinowski, and D. J. Thiele.** 1992. Expression of a yeast metallothionein gene family is activated by a single metalloregulatory transcription factor. Mol. Cell. Biol. **12:**3766–3775.
50. **Zhou, P., M. S. Szczypka, R. Young, and D. J. Thiele.** 1994. A system for gene cloning and manipulation in the yeast *Candida glabrata*. Gene **142:**135–140.
51. **Zhou, P., and D. J. Thiele.** 1991. Isolation of a metal-activated transcription factor gene from Candida glabrata by complementation in *Saccharomyces cerevisiae*. Proc. Natl. Acad. Sci. USA **88:**6112–6116.
52. **Zhou, P., and D. J. Thiele.** 1993. Rapid transcriptional autoregulation of a yeast metalloregulatory factor is essential for high-level copper detoxification. Genes Dev. **7:**1824–1835.
53. **Zieg, J., and M. I. Simon.** 1980. Analysis of the nucleotide sequence of an invertible controlling element. Proc. Natl. Acad. Sci. USA **77:**4196–4200.

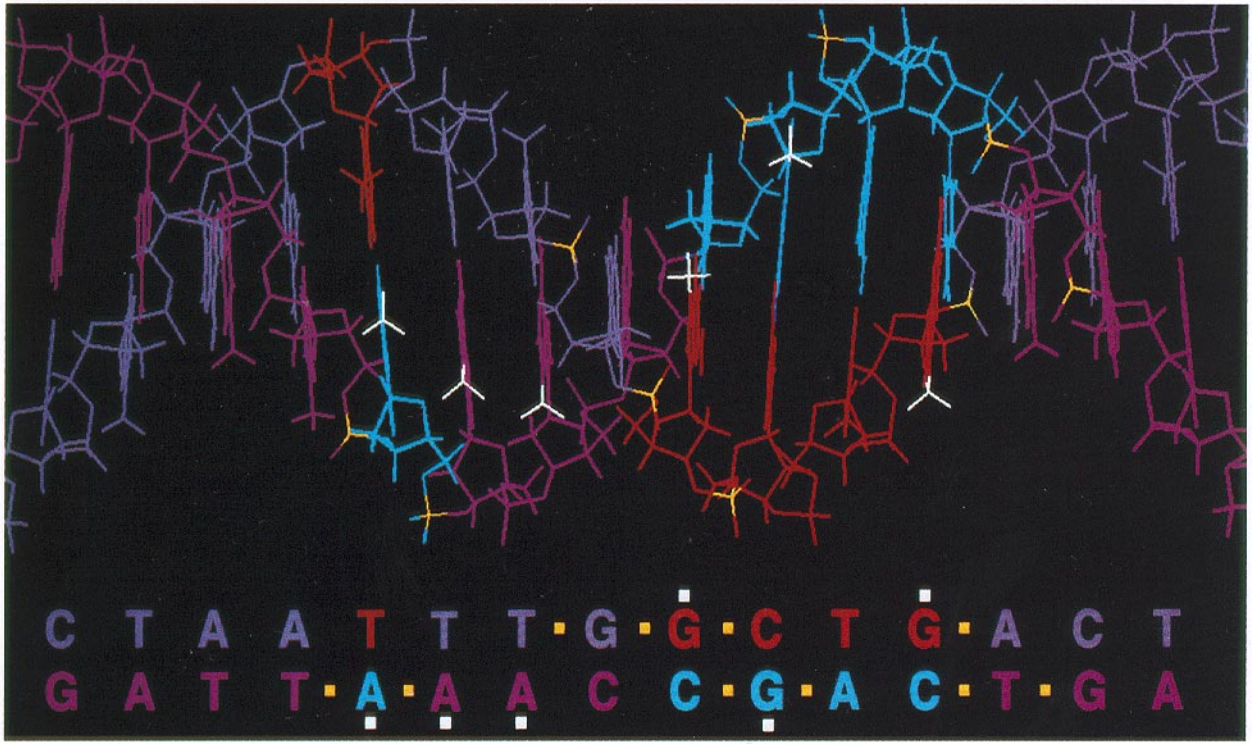
C T A A T T T · G · G · C T G · A C T
G A T T · A · A A C C · G · A C · T · G A